

Vector detection of AC magnetic fields by Nitrogen-Vacancy centers of single orientation in diamond

Pooja Lamba,^{1,*} Akshat Rana,^{1,*} Sougata Halder,² Siddharth Dhomkar,^{3,4} Dieter Suter,⁵ and Rama K. Kamineni^{1,†}

¹*Department of Physics, Bennett University, Greater Noida 201310, India*

²*Department of Physics, IIT Jodhpur, Jodhpur, India*

³*Department of Physics, IIT Madras, Chennai, India*

⁴*Center For Quantum Information, Communication And Computing, IIT Madras, Chennai, India*

⁵*Fakultät Physik, Technische Universität Dortmund, D-44221 Dortmund, Germany*

(Dated: August 21, 2023)

Nitrogen-Vacancy (NV) centers in diamond have useful properties for detecting both AC and DC magnetic fields with high sensitivity at nano-scale resolution. Vector detection of AC magnetic fields can be achieved by using NV centers having three different orientations. Here, we propose a method to achieve this by using NV centers of single orientation. In this method, a static magnetic field is applied perpendicular to the NV axis, leading to strong mixing of the $m_s = -1$ and 1 electron spin states. As a result, all three electron spin transitions of the triplet ground state have non-zero dipole moments, with each transition coupling to a single component of the magnetic field. This can be used to measure both strength and orientation of the applied AC field. To validate the technique, we perform a proof of principle experiment using a subset of ensemble NV centers in diamond, all having the same orientation.

I. INTRODUCTION

Sensitive detection of magnetic fields is an essential task in many areas of science, technology, and medicine. Sensors based on different techniques have been developed for this purpose [1–4]. Among these, sensors based on Nitrogen-Vacancy (NV) centers in diamond have the advantages of room-temperature operation and high-sensitivity detection with nano-scale resolution [5–7]. Additionally, NV centers are useful for detecting both AC and DC magnetic fields [8–15].

Sensitive detection of AC magnetic fields produced by spins and charges at micro- and nano-scales have interesting applications in magnetic resonance and condensed matter physics. Methods based on different technologies have been developed for this purpose [16–23]. In many cases, it is desirable to measure not only the magnitude, but also the orientation of the magnetic fields. Important examples where vector detection of AC fields is important include magnetic excitations and current distributions in materials [24]. Most of the existing methods for detecting AC magnetic fields in the microwave (MW) frequency range lack vector detection capabilities or nano-scale resolution.

Small sensor size, long-coherence times, and C_{3V} symmetry of NV centers can be beneficial for vector detection of DC and AC magnetic fields. Vector detection of DC and slow time-varying fields by using NV centers have been thoroughly investigated [25–32]. Here, we focus on vector detection of fields with frequency greater than 1 MHz. For small static magnetic fields, the quantization axis of NV centers is pointed along the NV axis.

The electron spin dipole moments, in general, are perpendicular to the quantization axis and hence only the components of the applied AC fields that are perpendicular to the quantization axis interact with the spin transitions of the center. Therefore, to achieve vector detection of AC fields using conventional technique, at least, three NV centers having varied orientations are essential. This has been demonstrated by using ensemble NV centers [33]. However, the requirement of multiple NV centers with different orientations puts restriction on the sensor size and limits its applicability for nano-scale imaging. Recently, vector detection of AC magnetic fields by a single NV center has been demonstrated by using a method known as "rotating-frame Rabi magnetometry" [34]. In this work, the components of the applied AC field have been measured by tuning the Rabi frequencies of NV spin transitions to different resonance conditions. However, this method requires that the Rabi frequencies of the electron spin transitions are comparable to their transition frequencies, which is a stringent prerequisite. A vector detection scheme using level anti-crossings of an NV center coupled to a first-shell ^{13}C nuclear spin has been reported in Ref. [35]. The anti-crossings used in this work occur when the energy level splitting due to Zeeman interaction of the NV electron spin is equal to the splitting due to hyperfine interaction of first-shell ^{13}C nuclear spin. The disadvantage of this method is that it requires a first-shell ^{13}C atom; probability of finding such a configuration is merely 3.3%. Moreover, the bandwidth of the sensor is very narrow.

NV centers with transverse magnetic field have been previously used for electric-field sensing [36], suppression of electron spin decoherence [35, 37], and magnetic field angle sensing [38].

Here, we propose and demonstrate a novel method for vector detection of AC magnetic fields via NV centers of single orientation, which exploits the energy level anti-

* These authors contributed equally to this work.

† koti.kamineni@gmail.com

crossing that occurs due to an application of the static magnetic field perpendicular to the NV axis. Particularly, for magnetic fields of strength up to few tens of mT, the eigenstates of the electron spin of the center at this level anti-crossing can be approximately written as $|0\rangle$, $\frac{|-1\rangle - |1\rangle}{\sqrt{2}}$, and $\frac{|-1\rangle + |1\rangle}{\sqrt{2}}$, where $|m_s\rangle = |0\rangle, |\pm 1\rangle$ refer to the eigenstates of the electron spin operator S_z and z is orientated along the symmetry axis of the NV center. All three transitions between these levels, including the transition in the $m_s = \pm 1$ subspace, have strong dipole moments and their directions are perpendicular to each other. Only the component of the applied AC field that is oriented parallel to the dipole moment can excite the corresponding transition. This can be used to measure both strength and orientation of the applied AC field. The amplitude of the vector components of the AC field can be measured by on-resonantly exciting each of the three transitions. The frequencies of these transitions can be tuned to match the frequency of the AC field by varying the strength of the static magnetic field.

This paper is arranged as follows - In section II, we describe the method, and in section III, we demonstrate the method experimentally by using an ensemble of identically oriented NV centers in diamond. Finally, in section IV we discuss and conclude.

II. METHODOLOGY

The NV center is a point defect in diamond with C_{3V} symmetry [39, 40]. It has spin-1 ground and excited states. Optical pumping causes polarization of its electron spin into the $m_s = 0$ state. Since the intensity of the fluorescence emitted by the center depends on its spin state, it is possible to read the spin state of the center optically. The Hamiltonian for the electron spin of the ground state of the NV center in an applied static magnetic field can be written as

$$\mathcal{H}_0 = DS_z^2 + \gamma_e B(\sin \theta S_x + \cos \theta S_z). \quad (1)$$

Here, we consider $h = 1$ and use frequency units for energy. $S_{x/y/z}$ represent the components of the spin-1 angular momentum operator. $D = 2870$ MHz is the zero-field splitting between the $|m_s\rangle = |0\rangle$ and $|\pm 1\rangle$ states. γ_e represent the gyromagnetic ratio of the electron spin. B and θ represent the strength and polar angle of the static magnetic field in a coordinate system whose Z-axis is aligned with the symmetry axis of the center, as shown in Fig. 1 (a). For $\theta \neq 0$, the X-axis is defined as the direction of the projection of the field into the plane perpendicular to the Z-axis.

The $|m_s\rangle = |\pm 1\rangle$ states, which are degenerate in zero magnetic field, split due to the Zeeman interaction and this splitting is proportional to the strength of the applied static magnetic field. When the field is applied parallel to the NV axis or at a small angle to it, m_s is a good quantum number and the eigenstates of the electron spin

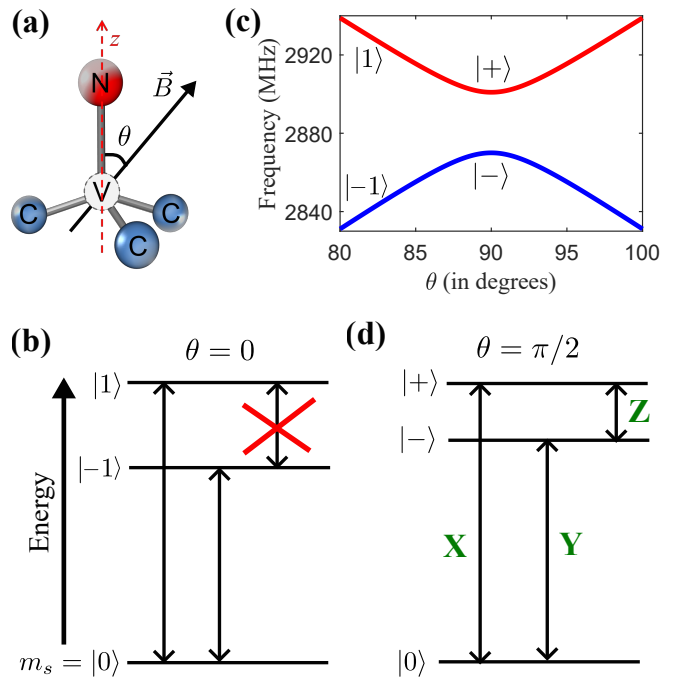


FIG. 1. (a) Schematic diagram of the NV center in diamond and the static magnetic field. (b) Energy level diagram of the ground state of the NV center and the allowed transitions between them when \vec{B} is oriented parallel to the NV axis. (c) Frequencies of energy levels of the $m_s = \pm 1$ subspace as a function of θ for $B = 10.7$ mT. (d) Energy level diagram when \vec{B} is oriented perpendicular to the NV axis. The transition labeled by Z has a dipole moment along the NV axis, the transition labeled by X has a dipole moment along the direction of \vec{B} , and the transition labeled by Y has a dipole moment perpendicular to both these directions.

are $|0\rangle$, $|-1\rangle$, and $|1\rangle$. As shown in Fig. 1(b), the transitions $|0\rangle \leftrightarrow |-1\rangle$ and $|0\rangle \leftrightarrow |1\rangle$ are allowed and the transition between the states $|-1\rangle$ and $|1\rangle$ is forbidden. The transition dipole moments of the allowed transitions are oriented perpendicular to the NV axis and, thus, can be excited by components of resonant microwave fields that are oriented perpendicular to the NV axis.

When the angle between the NV axis and the static magnetic field is close to $\pi/2$, there is a strong mixing between the states $|m_s\rangle = |-1\rangle$ and $|1\rangle$. As shown in Fig. 1(c), the plot of energy levels versus angle θ shows anti-crossing at $\theta = \pi/2$. For magnetic fields of strength up to few tens of mT, the eigenstates of the electron spin at $\theta = \pi/2$ can be approximately written as $|0\rangle$, $|-\rangle$, and $|+\rangle$, where $|-\rangle$ and $|+\rangle$ are defined as $\frac{1}{\sqrt{2}}(|-1\rangle - |1\rangle)$ and $\frac{1}{\sqrt{2}}(|-1\rangle + |1\rangle)$, respectively. The separation between the states $|-\rangle$ and $|+\rangle$ is of the order of $\frac{(\gamma_e B)^2}{D}$. All three transitions between the states $|0\rangle$, $|-\rangle$, and $|+\rangle$ are allowed and have strong dipole moments (Fig. 1(d)). Most importantly, the orientations of dipole moments of these transitions are orthogonal to each other. The dipole mo-

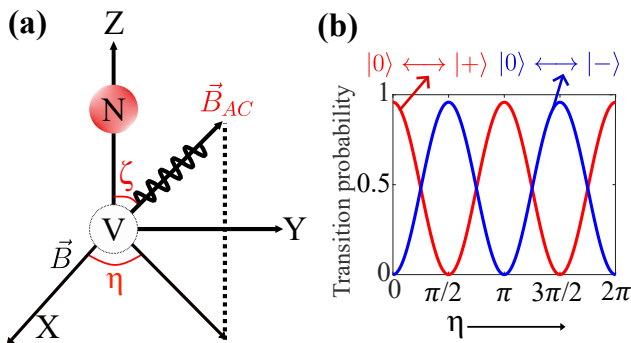


FIG. 2. (a) Coordinate system with static and AC magnetic field orientations. (b) Transition probabilities of $|0\rangle \leftrightarrow |+\rangle$ and $|0\rangle \leftrightarrow |-\rangle$ transitions as a function of η for $\theta = \pi/2$.

ment of the transition between the states $|-\rangle$ and $|+\rangle$ is parallel to the NV axis, the dipole moment of the transition between the states $|0\rangle$ and $|+\rangle$ is along the direction of the magnetic field, and the dipole moment of the transition between the states $|0\rangle$ and $|-\rangle$ is oriented perpendicular to both these directions. In the coordinate system defined earlier in this section, $|\langle -|S_z|+\rangle| \approx 1$, $|\langle 0|S_x|+\rangle| \approx 1$, and $|\langle 0|S_y|-\rangle| \approx 1$, while all other matrix elements are close to zero. This can be utilized for vector detection of magnetic fields [15]. The highest sensitivity is achieved for AC fields that are on-resonance with these transitions.

A linearly polarized AC magnetic field can be expressed as

$$\vec{B}_{AC} = B_{AC}(\sin \zeta \cos \eta \hat{x} + \sin \zeta \sin \eta \hat{y} + \cos \zeta \hat{z}) \cos(\omega t + \varphi), \quad (2)$$

where B_{AC} , ζ , and η are the strength, polar, and azimuthal angles of the field, respectively. ω and φ are the angular frequency and phase of the field. A schematic representation of \vec{B}_{AC} , and the angles ζ and η are given in Fig. 2(a). The Hamiltonian corresponding to the interaction of the AC field with the electron spin of the NV center can be written as

$$\mathcal{H}_{AC} = \gamma_e \vec{B}_{AC} \cdot \vec{S}. \quad (3)$$

The purpose of this paper is to determine the parameters B_{AC} , ζ , and η of the AC field from experimental measurements. As shown in Fig. 2(b), the probabilities of the transitions $|0\rangle \leftrightarrow |-\rangle$ and $|0\rangle \leftrightarrow |+\rangle$ have sinusoidal dependence on the angle η between the static field and the transverse component of the AC field. When $\eta = 0$ ($\eta = \pi/2$), the probability of the transition $|0\rangle \leftrightarrow |-\rangle$ ($|0\rangle \leftrightarrow |+\rangle$) is close to zero and the probability of $|0\rangle \leftrightarrow |+\rangle$ ($|0\rangle \leftrightarrow |-\rangle$) is close to one. Therefore, by comparing the experimental amplitudes or Rabi frequencies of the aforementioned transitions for a fixed transverse orientation of the static field, we can determine the angle η . Once η is known, B_{AC} and ζ can

be determined by comparing the Rabi frequencies of the transition $|-\rangle \leftrightarrow |+\rangle$ and any one of the two transitions $|0\rangle \leftrightarrow |-\rangle$ and $|0\rangle \leftrightarrow |+\rangle$. When the frequency of the applied AC field matches the frequency of the transitions, whose dipole moment is along the direction of the field, it induces transitions, which may be observed as a drop in the fluorescence emitted by the NV centers under optical illumination. This effect is known as Optical Detection of Magnetic Resonance (ODMR) [41, 42].

III. PROOF-OF-PRINCIPLE EXPERIMENTS

The experiments were performed on a home-built confocal microscope setup equipped with a 532 nm laser for off-resonant excitation of optical transitions, and radio-frequency (RF) and MW electronic circuits for resonant excitation of electron spin transitions. A CVD grown single crystal diamond with a nitrogen concentration of 800 ppb was used. There were hundreds of NV centers within the excitation volume of the confocal microscope. The AC magnetic fields, whose vector detection we were trying to achieve, was generated by a current through a 25 μm copper wire attached to the diamond surface. This work required precise orientation of the static magnetic field with respect to the NV axis and it was achieved by using a permanent magnet attached to two rotational stages whose axes were orthogonal to each other and crossed at the site of the diamond crystal. NV centers of all four possible orientations that were within the confocal spot were excited simultaneously by the laser and contributed to the total detected fluorescence. However, in the ODMR experiments, the frequency of the applied field selects only one specific orientation.

As described in the previous section, we determine η , the angle between the transverse component of the AC field and the static magnetic field. Specifically, Fig. 1(d) illustrates that when the static magnetic field is oriented perpendicular to the NV axis, the transition between the states $|0\rangle$ and $|+\rangle$ can only be excited by a component of the AC field that is parallel to the static magnetic field. Likewise, the transition between the states $|0\rangle$ and $|-\rangle$ can be excited by a component of the AC field that is perpendicular to both static field and NV axis. In our experimental setup, the direction of the applied AC field is fixed, but we can change the direction of the static magnetic field. We recorded ODMR spectra by applying a static magnetic field of strength 10.7 mT at different orientations in the plane perpendicular to the NV axis. Fig. 3 summarizes the results. When $\eta = 0$, the ODMR consists of only one peak at 2932 MHz corresponding to the $|0\rangle \leftrightarrow |+\rangle$ transition. The other peak at 2900 MHz corresponding to the transition $|0\rangle \leftrightarrow |-\rangle$ has negligible intensity. Conversely, when $\eta = \pi/2$, the peak at 2932 MHz is of negligible intensity compared to the peak at 2900 MHz. When $\eta = \pi/4$, as shown in Fig. 3(c), both peaks are of equal intensity. In other words, when the static magnetic field is aligned with the transverse com-

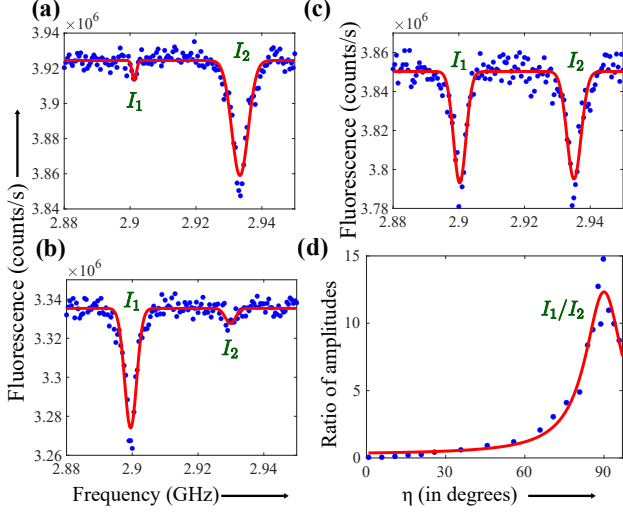


FIG. 3. ODMR spectra for different orientations of the static magnetic field in the plane perpendicular to the NV axis, (a) $\eta = 0$, (b) $\eta = \pi/2$, (c) $\eta = \pi/4$. Blue dots represent experimental data and red lines are Gaussian fits of these data. (d) Ratio of amplitudes, I_1/I_2 as a function of η . Blue dots represent the ratio of amplitudes determined from the ODMR spectra and the red line represents a fit of these data to the expression $a \frac{b}{(\eta - \eta_0)^2 + b^2} + c$, where $\eta_0 = 90^\circ (\pm 0.9)$.

ponent of the AC field, the transition $|0\rangle \leftrightarrow |-\rangle$ has minimum intensity and the transition $|0\rangle \leftrightarrow |+\rangle$ has maximum intensity. So, we can determine the direction of the transverse component of the AC field by simply rotating the static magnetic field in the plane perpendicular to the NV axis and look for the direction at which the transition $|0\rangle \leftrightarrow |-\rangle$ has minimum intensity and the transition $|0\rangle \leftrightarrow |+\rangle$ has maximum intensity. The ratio of intensities of these two transitions as a function of η is given in Fig. 3(d). The maximum of this ratio corresponds to $\eta = \pi/2$. From this, we are able to determine the direction of the transverse component of the AC field with an uncertainty $\pm 0.9^\circ$. Alternatively, one can also determine this at a given magnetic field orientation in the transverse plane by comparing the Rabi frequencies of the two transitions.

As mentioned in the last section, B_{AC} , the strength of the applied AC field and ζ , the angle between the NV axis and the direction of the AC field can be determined from the measured Rabi frequencies of the transitions, $|0\rangle \leftrightarrow |-\rangle$ and $|-\rangle \leftrightarrow |+\rangle$ for a fixed value of η . The Rabi oscillations of the transition $|0\rangle \leftrightarrow |-\rangle$ can be straightforwardly measured by using the pulse sequence given in Fig. 4(b) and the result is shown in Fig. 4(d).

Laser illumination doesn't create population difference between the states $|-\rangle$ and $|+\rangle$ and also these states cannot be distinguished directly from the intensity of the fluorescence emitted by the NV centers. So, to measure the Rabi oscillations of the transition $|-\rangle \leftrightarrow |+\rangle$, the pulse sequence given in Fig. 4(c) is used. First, the

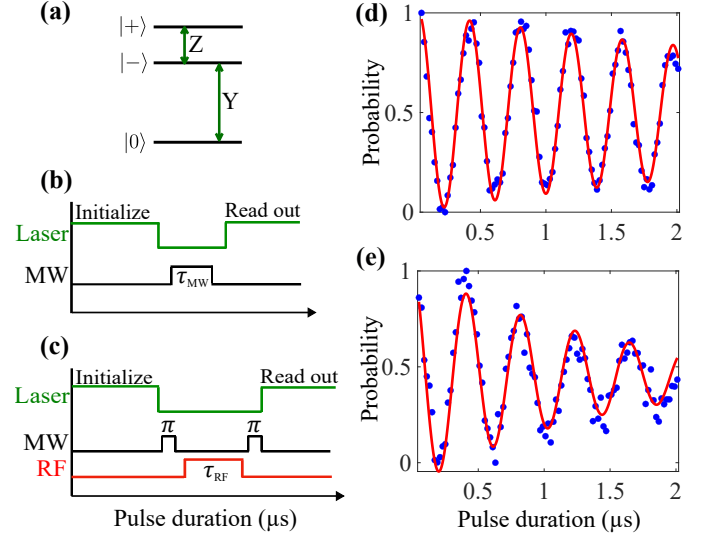


FIG. 4. Rabi oscillations and the pulse sequences. (a) Electron spin energy level diagram displaying the transitions whose Rabi oscillations are measured. (b) and (c) represent the pulse sequences, and (d) and (e) are the resultant Rabi oscillations of the transitions $|0\rangle \leftrightarrow |-\rangle$ and $|-\rangle \leftrightarrow |+\rangle$ respectively. MW and RF in (b) and (c) refer to the frequencies of the transitions $|0\rangle \leftrightarrow |-\rangle$ and $|-\rangle \leftrightarrow |+\rangle$, which are 2900 MHz and 32 MHz respectively. In (d) and (e), blue dots represent experimental data and red lines represent fits of this data to the expression $a \cos(2\pi\nu t) \exp(-t/T_R) + c$. $\nu = 2.57 (\pm 0.01)$ and $2.42 (\pm 0.02)$ MHz, and $T_R = 5 (\pm 1.7)$ and $1.4 (\pm 0.3)$ μs for (d) and (e) respectively.

state $|0\rangle$ is populated by a laser pulse and this population is transferred to the $|-\rangle$ state by a microwave π -pulse. This creates population difference between the states $|-\rangle$ and $|+\rangle$. For the actual Rabi experiment, the transition $|-\rangle \leftrightarrow |+\rangle$ is driven on-resonance by an RF pulse with a frequency of 32 MHz and variable duration. The resulting dynamics are measured by transferring the population from $|-\rangle$ to $|0\rangle$ by the second microwave π -pulse and reading it out by applying the second laser pulse. The corresponding Rabi oscillations are shown in Fig. 4(e).

The expressions relating the Rabi frequencies and the corresponding transition amplitudes can be written as

$$\sqrt{2} \frac{\gamma_e}{2\pi} B_{MW} \sin \zeta \cos \eta |\langle 0|S_x|+\rangle| = R_{0+}, \quad (4)$$

$$\sqrt{2} \frac{\gamma_e}{2\pi} B_{MW} \sin \zeta \sin \eta |\langle 0|S_y|-\rangle| = R_{0-}, \quad (5)$$

$$\sqrt{2} \frac{\gamma_e}{2\pi} B_{RF} \cos \zeta |\langle -|S_z|+\rangle| = R_{-+}. \quad (6)$$

Here, B_{MW} and B_{RF} represent the amplitudes of the AC field at frequencies 2900 MHz and 32 MHz respectively. $R_{0+} = 3.15 (\pm 0.01)$ MHz, $R_{0-} = 2.57 (\pm 0.01)$ MHz and $R_{-+} = 2.42 (\pm 0.02)$ MHz are the measured Rabi frequencies of the transitions $|0\rangle \leftrightarrow |+\rangle$, $|0\rangle \leftrightarrow |-\rangle$

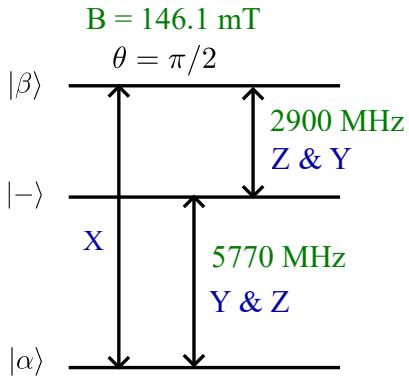


FIG. 5. Energy level diagram of the electron spin in the NV center for $B = 146.1$ mT and $\theta = \pi/2$. Here, $|\alpha\rangle = 0.82|0\rangle - 0.58|+\rangle$ and $|\beta\rangle = 0.82|+\rangle + 0.58|0\rangle$. The labels X, Y and Z represent the orientation of the dipole moment of the corresponding transitions.

and $|- \rangle \longleftrightarrow |+\rangle$ respectively. The ratio $\frac{B_{RF}}{B_{MW}} = 0.23$ has been determined from the measured power levels. By substituting all the extracted parameters and solving for B_{MW} , B_{RF} , ζ and η , we obtain them as $B_{MW} = 2.85 (\pm 0.01)$ G, $B_{RF} = 0.66 (\pm 0.01)$ G, $\zeta = 21.6^\circ (\pm 0.2)$ and $\eta = 38.8^\circ (\pm 0.1)$.

The sensitivity of the magnetic field measurement can be calculated by using the formula [43–45]

$$\eta_B = \delta B \sqrt{nT}, \quad (7)$$

where δB is the uncertainty in the measurement of the AC magnetic field, n is the total number of experiments, and T is the sensing time in each experiment. From the fit of the Rabi oscillations, we estimate $\eta_B \approx 1 \mu\text{T}/\sqrt{Hz}$, which is similar to the previously reported sensitivity values [33, 34].

IV. DISCUSSION AND CONCLUSION

The experimental demonstration of the method presented in the last section uses an AC field of two different frequencies for the vector detection. However, when vector detection of an arbitrary AC field is performed, it may not always be possible to tune its frequency. The proposed method can be used for vector detection of an AC field of single frequency, but it requires application of a static magnetic field of two different strengths; one of them is greater than 100 mT, which is beyond the field strength that our current experimental setup can produce at the site of diamond crystal. Nevertheless, we now discuss the procedure to perform vector detection at a single frequency - as a specific example, we choose a frequency of 2900 MHz. The angle η or the direction of the transverse component of the AC field can be determined by applying a static magnetic field of strength 10.6 mT in the plane perpendicular to the NV axis. The fre-

quency of the transition $|0\rangle \longleftrightarrow |- \rangle$ at this field is 2900 MHz. The orientation of the static field at which this transition has the lowest intensity is the direction of the transverse component of the AC field. To determine the magnitude B_{AC} and the angle ζ , first we can measure the Rabi frequency of the transition $|0\rangle \longleftrightarrow |- \rangle$ in the static field of 10.6 mT oriented in the transverse plane with $\eta = \pi/2$. Next, a field of 146.1 mT can be applied in the transverse plane, with $\eta = 0$. This field mixes the states $|0\rangle$ and $|+\rangle$ and the new eigenstates are $|\alpha\rangle$, $|- \rangle$, and $|\beta\rangle$, where $|\alpha\rangle = 0.82|0\rangle - 0.58|+\rangle$ and $|\beta\rangle = 0.82|+\rangle + 0.58|0\rangle$. The state $|- \rangle$ doesn't mix with the other states, as it is an eigenstate of both, the S_z^2 and S_x operators. The energy level diagram for this field orientation is given in Fig. 5. The frequency of the transition $|- \rangle \longleftrightarrow |\beta\rangle$ is 2900 MHz and it can be excited by the Y- and Z-components of the AC field. Since we already know the direction of the transverse component of the AC field, the Y-component can be made equal to zero by orienting the static magnetic field along this direction. Note that X-axis is defined as the direction of the static field. So, for $\eta = 0$, the transition $|- \rangle \longleftrightarrow |\beta\rangle$ can only be excited by the Z-component of the AC field. By measuring the Rabi frequency of this transition and using it in combination with the Rabi frequency of the transition $|0\rangle \longleftrightarrow |- \rangle$ at the field of 10.6 mT, we can determine the parameters, B_{AC} and ζ . An important point to note here is that the mixing between the states $|0\rangle$ and $|+\rangle$ can decrease the polarization of the electron spin under optical pumping and that in turn can decrease the ODMR contrast.

The aforementioned procedure is intended for vector detection of AC fields of frequency greater than 2870 MHz as this is the lowest frequency for the transitions $|0\rangle \longleftrightarrow |- \rangle$ and $|0\rangle \longleftrightarrow |+\rangle$. Now, we discuss the protocol for vector detection of fields in the frequency range 1 - 2870 MHz. The frequency of the transition $|- \rangle \longleftrightarrow |\beta\rangle$ is in the frequency range 1 - 2870 MHz for static fields of strength 0 - 145 mT oriented perpendicular to the NV axis. This transition can be excited by only the Z-component or by Z- and Y-components of the applied AC fields depending upon the strength and orientation of the static field in the transverse plane of the NV center. When a static field of strength 0 - 100 mT is applied parallel to the NV axis, the frequency of the transition $|0\rangle \longleftrightarrow |- \rangle$ is in the range 1 - 2870 MHz and it can only be excited by the transverse components of the AC field. So, from the Rabi frequencies of the transitions $|- \rangle \longleftrightarrow |\beta\rangle$ and $|0\rangle \longleftrightarrow |- \rangle$ at appropriate static magnetic fields, we can determine the strength of the AC field (B_{AC}) and the angle between the NV axis and the AC field (ζ). The Rabi frequency of the transition $|- \rangle \longleftrightarrow |\beta\rangle$ is proportional to $|\cos \zeta \langle -|S_z|\beta\rangle + \sin \zeta \sin \eta \langle -|S_y|\beta\rangle|$, which is minimum at $\eta = 0$ and maximum at $\eta = \pi/2$ for a fixed value of ζ . So, by measuring the Rabi frequency of this transition for different orientations of static field in the transverse plane, we can determine η , the azimuthal angle of the AC field. However, the amplitude of variation in these

Rabi frequencies is proportional to the matrix element $|\langle -|S_y|\beta\rangle|$, which is very small for static fields of strength less than 10 mT. Hence, experimental determination of η for AC fields of frequency less than 30 MHz may be difficult.

In conclusion, we have proposed and experimentally demonstrated a method for vector detection of AC fields by using NV centers having single orientation. The method is undemanding relative to the conventional technique and is applicable for wide frequency range. Though the method is demonstrated by using an ensemble of NV centers with a single orientation, it is equally applicable for an ensemble consisting only of a single NV center. Since this method does not require NV centers of multiple orientations, it can be used for vector imaging of AC fields with nano-scale resolution. In particular, this method is suitable for vector AC field imaging by using single NV centers of diamond nanopillar probes attached to atomic force microscope [12, 46]. This work will also be useful for optimal control of quantum registers based on multiple dipolar coupled NV centers having different orientations in diamond. In such registers, it is not pos-

sible to align static magnetic field with the NV axes of all the centers. Designing time-optimal quantum gates to the electron and ^{13}C nuclear spin qubits of misaligned NV centers requires accurate knowledge of the internal as well as the RF and MW control field Hamiltonians. The vector AC field detection scheme demonstrated in this work is useful for precise determination of the control field Hamiltonian.

V. ACKNOWLEDGEMENTS

A.R. and R.K.K. acknowledge support from Department of Science & Technology - Science & Engineering Research Board (DST-SERB), India through grant no. SRG/2020/000765. S.D. thanks Indian Institute of Technology, Madras, India for the seed funding. S.D. acknowledges the financial support by the Mphasis F1 Foundation given to the Centre for Quantum Information, Communication, and Computing (CQuICC).

-
- [1] D. Budker and M. Romalis, Optical magnetometry, *Nature Physics* **3**, 227 (2007).
 - [2] M. Vengalattore, J. M. Higbie, S. R. Leslie, J. Guzman, L. E. Sadler, and D. M. Stamper-Kurn, High-resolution magnetometry with a spinor bose-einstein condensate, *Phys. Rev. Lett.* **98**, 200801 (2007).
 - [3] G. S. Waters and P. D. Francis, A nuclear magnetometer, *Journal of Scientific Instruments* **35**, 88 (1958).
 - [4] R. L. Fagaly, Superconducting quantum interference device instruments and applications, *Review of Scientific Instruments* **77**, 101101 (2006).
 - [5] R. Schirhagl, K. Chang, M. Loretz, and C. L. Degen, Nitrogen-vacancy centers in diamond: Nanoscale sensors for physics and biology, *Annual Review of Physical Chemistry* **65**, 83 (2014).
 - [6] L. Rondin, J.-P. Tetienne, T. Hingant, J.-F. Roch, P. Maletinsky, and V. Jacques, Magnetometry with nitrogen-vacancy defects in diamond, *Reports on Progress in Physics* **77**, 056503 (2014).
 - [7] S. Hong, M. S. Grinolds, L. M. Pham, D. L. Sage, L. Luan, R. L. Walsworth, and A. Yacoby, Nanoscale magnetometry with nv centers in diamond, *MRS Bulletin* **38**, 155 (2013).
 - [8] G. Balasubramanian, I. Chan, R. Kolesov, M. Al-Hmoud, J. Tisler, C. Shin, C. Kim, A. Wojcik, P. R. Hemmer, A. Krueger, *et al.*, Nanoscale imaging magnetometry with diamond spins under ambient conditions, *Nature* **455**, 648 (2008).
 - [9] C. L. Degen, Scanning magnetic field microscope with a diamond single-spin sensor, *Applied Physics Letters* **92**, 243111 (2008).
 - [10] J. R. Maze, P. L. Stanwix, J. S. Hodges, S. Hong, J. M. Taylor, P. Cappellaro, L. Jiang, M. V. G. Dutt, E. Togan, A. S. Zibrov, A. Yacoby, R. L. Walsworth, and M. D. Lukin, Nanoscale magnetic sensing with an individual electronic spin in diamond, *Nature* **455**, 644 (2008).
 - [11] T. Staudacher, F. Shi, S. Pezzagna, J. Meijer, J. Du, C. A. Meriles, F. Reinhard, and J. Wrachtrup, Nuclear magnetic resonance spectroscopy on a (5-nanometer)³ sample volume, *Science* **339**, 561 (2013).
 - [12] P. Appel, M. Ganzhorn, E. Neu, and P. Maletinsky, Nanoscale microwave imaging with a single electron spin in diamond, *New Journal of Physics* **17**, 112001 (2015).
 - [13] J. M. Boss, K. S. Cujia, J. Zopes, and C. L. Degen, Quantum sensing with arbitrary frequency resolution, *Science* **356**, 837 (2017).
 - [14] S. Schmitt, T. Gefen, F. M. Stürner, T. Uden, G. Wolff, C. Müller, J. Scheuer, B. Naydenov, M. Markham, S. Pezzagna, J. Meijer, I. Schwarz, M. Plenio, A. Retzker, L. P. McGuinness, and F. Jelezko, Submillihertz magnetic spectroscopy performed with a nanoscale quantum sensor, *Science* **356**, 832 (2017).
 - [15] J. Zhang and D. Suter, Single nv centers as sensors for radio-frequency fields, *Phys. Rev. Res.* **5**, L022026 (2023).
 - [16] R. C. Black, F. C. Wellstood, E. Dantsker, A. H. Miklich, D. Koelle, F. Ludwig, and J. Clarke, Imaging radio-frequency fields using a scanning squid microscope, *Applied Physics Letters* **66**, 1267 (1995).
 - [17] V. Agrawal, P. Neuzil, and D. W. van der Weide, A microfabricated tip for simultaneous acquisition of sample topography and high-frequency magnetic field, *Applied Physics Letters* **71**, 2343 (1997).
 - [18] S.-C. Lee, C. P. Vlahacos, B. J. Feenstra, A. Schwartz, D. E. Steinhauer, F. C. Wellstood, and S. M. Anlage, Magnetic permeability imaging of metals with a scanning near-field microwave microscope, *Applied Physics Letters* **77**, 4404 (2000).
 - [19] P. Böhi, M. F. Riedel, T. W. Hänsch, and P. Treutlein, Imaging of microwave fields using ultracold atoms, *Applied Physics Letters* **97**, 051101 (2010).

- [20] P. Böhi and P. Treutlein, Simple microwave field imaging technique using hot atomic vapor cells, *Applied Physics Letters* **101**, 181107 (2012).
- [21] C. F. Ockeloen, R. Schmied, M. F. Riedel, and P. Treutlein, Quantum metrology with a scanning probe atom interferometer, *Phys. Rev. Lett.* **111**, 143001 (2013).
- [22] T. van der Sar, F. Casola, R. Walsworth, and A. Yacoby, Nanometre-scale probing of spin waves using single electron spins, *Nature Communications* **6**, 7886 (2015).
- [23] K. Chang, A. Eichler, J. Rhensius, L. Lorenzelli, and C. L. Degen, Nanoscale imaging of current density with a single-spin magnetometer, *Nano Letters* **17**, 2367 (2017).
- [24] F. Casola, T. van der Sar, and A. Yacoby, Probing condensed matter physics with magnetometry based on nitrogen-vacancy centres in diamond, *Nature Reviews Materials* **3**, 17088 (2018).
- [25] B. J. Maertz, A. P. Wijnheijmer, G. D. Fuchs, M. E. Nowakowski, and D. D. Awschalom, Vector magnetic field microscopy using nitrogen vacancy centers in diamond, *Applied Physics Letters* **96**, 092504 (2010).
- [26] C. Zhang, H. Yuan, N. Zhang, L. Xu, J. Zhang, B. Li, and J. Fang, Vector magnetometer based on synchronous manipulation of nitrogen-vacancy centers in all crystal directions, *Journal of Physics D: Applied Physics* **51**, 155102 (2018).
- [27] H. Clevenson, L. M. Pham, C. Teale, K. Johnson, D. Englund, and D. Braje, Robust high-dynamic-range vector magnetometry with nitrogen-vacancy centers in diamond, *Applied Physics Letters* **112**, 252406 (2018).
- [28] J. M. Schloss, J. F. Barry, M. J. Turner, and R. L. Walsworth, Simultaneous broadband vector magnetometry using solid-state spins, *Phys. Rev. Appl.* **10**, 034044 (2018).
- [29] H. Zheng, Z. Sun, G. Chatzidrosos, C. Zhang, K. Nakamura, H. Sumiya, T. Ohshima, J. Isoya, J. Wrachtrup, A. Wickenbrock, and D. Budker, Microwave-free vector magnetometry with nitrogen-vacancy centers along a single axis in diamond, *Phys. Rev. Appl.* **13**, 044023 (2020).
- [30] D. Broadway, S. Lillie, S. Scholten, D. Rohner, N. Dontschuk, P. Maletinsky, J.-P. Tetienne, and L. Hollenberg, Improved current density and magnetization reconstruction through vector magnetic field measurements, *Phys. Rev. Appl.* **14**, 024076 (2020).
- [31] T. Weggler, C. Ganslmayer, F. Frank, T. Eilert, F. Jelezko, and J. Michaelis, Determination of the three-dimensional magnetic field vector orientation with nitrogen vacancy centers in diamond, *Nano Letters* **20**, 2980 (2020).
- [32] B. Chen, X. Hou, F. Ge, X. Zhang, Y. Ji, H. Li, P. Qian, Y. Wang, N. Xu, and J. Du, Calibration-free vector magnetometry using nitrogen-vacancy center in diamond integrated with optical vortex beam, *Nano Letters* **20**, 8267 (2020).
- [33] P. Wang, Z. Yuan, P. Huang, X. Rong, M. Wang, X. Xu, C. Duan, C. Ju, F. Shi, and J. Du, High-resolution vector microwave magnetometry based on solid-state spins in diamond, *Nature Communications* **6**, 6631 (2015).
- [34] G. Wang, Y.-X. Liu, Y. Zhu, and P. Cappellaro, Nanoscale vector ac magnetometry with a single nitrogen-vacancy center in diamond, *Nano Letters* **21**, 5143 (2021).
- [35] K. R. K. Rao and D. Suter, Level anti-crossings of a nitrogen-vacancy center in diamond: decoherence-free subspaces and 3d sensors of microwave magnetic fields, *New Journal of Physics* **22**, 103065 (2020).
- [36] F. Dolde, H. Fedder, M. W. Doherty, T. Nobauer, F. Rempp, G. Balasubramanian, T. Wolf, F. Reinhard, L. C. L. Hollenberg, F. Jelezko, and J. Wrachtrup, Electric-field sensing using single diamond spins, *Nature Physics* **7**, 459 (2011).
- [37] C. S. Shin, C. E. Avalos, M. C. Butler, H.-J. Wang, S. J. Seltzer, R.-B. Liu, A. Pines, and V. S. Bajaj, Suppression of electron spin decoherence of the diamond nv center by a transverse magnetic field, *Phys. Rev. B* **88**, 161412 (2013).
- [38] Z. Qiu, U. Vool, A. Hamo, and A. Yacoby, Nuclear spin assisted magnetic field angle sensing, *npj Quantum Information* **7**, 39 (2021).
- [39] M. W. Doherty, N. B. Manson, P. Delaney, F. Jelezko, J. Wrachtrup, and L. C. Hollenberg, The nitrogen-vacancy colour centre in diamond, *Physics Reports* **528**, 1 (2013).
- [40] D. Suter and F. Jelezko, Single-spin magnetic resonance in the nitrogen-vacancy center of diamond, *Progress in Nuclear Magnetic Resonance Spectroscopy* **98-99**, 50 (2017).
- [41] F. Bitter, The optical detection of radiofrequency resonance, *Phys. Rev.* **76**, 833 (1949).
- [42] D. Suter, Optical detection of magnetic resonance, *Magnetic Resonance* **1**, 115 (2020).
- [43] J. M. Taylor, P. Cappellaro, L. Childress, L. Jiang, D. Budker, P. R. Hemmer, A. Yacoby, R. Walsworth, and M. D. Lukin, High-sensitivity diamond magnetometer with nanoscale resolution, *Nature Physics* **4**, 810 (2008).
- [44] R. S. Schoenfeld and W. Harneit, Real time magnetic field sensing and imaging using a single spin in diamond, *Phys. Rev. Lett.* **106**, 030802 (2011).
- [45] A. Dréau, M. Lesik, L. Rondin, P. Spinicelli, O. Arcizet, J.-F. Roch, and V. Jacques, Avoiding power broadening in optically detected magnetic resonance of single nv defects for enhanced dc magnetic field sensitivity, *Phys. Rev. B* **84**, 195204 (2011).
- [46] P. Maletinsky, S. Hong, M. S. Grinolds, B. Hausmann, M. D. Lukin, R. L. Walsworth, M. Loncar, and A. Yacoby, A robust scanning diamond sensor for nanoscale imaging with single nitrogen-vacancy centres, *Nature Nanotechnology* **7**, 320 (2012).